Engineering Science and Technology, an International Journal 19 (2016) 1283–1298

HOSTED BY

ELSEVIER

Contents lists available at ScienceDirect

Engineering Science and Technology, an International Journal

journal homepage: www.elsevier.com/locate/jestch

Full Length Article

A comparative study of mixed convection and its effect on partially active thermal zones in a two sided lid-driven cavity filled with nanofluid

Sumit Malik, A.K. Nayak *

Department of Mathematics, Indian Institute Technology of Roorkee, Roorkee 247667, India

ARTICLE INFO

Article history:
Received 12 January 2016
Revised 19 February 2016
Accepted 22 February 2016
Available online 12 April 2016

Keywords:
Mixed convection
Nanofluid
Lid-driven cavity
Flow and heat transfer
Finite volume method
SIMPLE algorithm

ABSTRACT

In the present study, a two sided lid-driven mixed convection nanofluid flow with discrete heat sources have been numerically investigated. A two dimensional computational visualization technique is used to study the flow behavior using four different cases; depending on the direction of moving vertical walls with fixed upper and lower walls. Two discrete heat sources of equal lengths are taken on the lower wall and the rest of it is kept insulated. The other walls are kept at constant low temperature. The effect of flow governing parameters such as Reynolds number $1 \leqslant Re \leqslant 100$, Richardson number $0.1 \leqslant Ri \leqslant 10$ and solid volume fraction $0.0 \leqslant \phi \leqslant 0.2$ with Prandtl number $Pr = 6.2$ is studied to understand the fluid flow pattern and the heat transfer effect using isotherms and average Nusselt number.

1. Introduction

Nowadays a study of mixed convection and heat transfer in enclosures is invariably encountered in many industrial heating or cooling applications including cooling of electronic devices, solar collectors, float glass production, drying technologies, chemical processing equipments, etc. and is of great interest for researchers. This type of fluid flow and heat transfer represents a complicated flow phenomena due to the movement of one or more walls which involves forced convection and the temperature difference causing secondary buoyancy driven flow. Fluid flow and heat transfer in square or rectangular cavities driven by shear and buoyancy effects have been studied extensively. In the application point of view an enormous amount of heat needs to be emitted from a considerably small surface, the coolant should have more effectual heat transfer properties. But due to the low thermal conductivity the conventional heat transfer fluids such as water, ethylene glycol mixture has foremost limitation in enhancing the heat transfer performance and the compactness of many industrial and engineering electronic devices. Heat transfer capabilities of the conventional fluids can be enhanced effectively using nanofluids, owing to their high thermal conductivity and better stability properties. To improve thermal conductivity, nano-scale metallic particles are suspended within the fluid. The resulting mixture is referred to as nanofluid that possesses a significant larger thermal conductivity compared to the conventional fluids [1].

In the last several years, an extensive numerical, analytical and experimental study has been done on the problem of natural and mixed convection heat transfer in cavities filled with nanofluid. The natural convection problem in a differentially heated square cavity is first numerically studied by Khanafer et al. [2], with the consideration of dispersion effect. In this work, a better model for nanofluids is developed by determining the dispersion coefficient experimentally. The effect of dispersion element in a nanofluid is discussed by Khaled and Vafai [3]. The volume fraction distribution is governed by the properties of dispersive elements combined with the flow parameters such as Reynolds number and Prandtl number for optimum heat transfer. In the case of uniform flow the maximum Nusselt number distribution is found to be 21% higher than that of the dispersed distributed element flow. Maiga et al. [4] numerically studied nanofluids in a uniformly heated tube for laminar and turbulent flow. They tried to correlate the numerical results with the experimental data and observed that for increase of Reynolds number, the heat transfer effect is increasing due to the presence of nanoparticles and becomes more important in the case of turbulent flow regimes. Tiwari and Das [5] numerically simulated the problem of mixed convection in two

* Corresponding author.
E-mail address: ameeyakumar@gmail.com (A.K. Nayak).
Peer review under responsibility of Karabuk University.

http://dx.doi.org/10.1016/j.jestch.2016.02.008
2215-0986/

Nomenclature

C_p	specific heat capacity (J/K)
g	gravitational acceleration (m/s^2)
k	thermal conductivity (W/mK)
Pr	Prandtl number
Re	Reynolds number
Gr	Grashof Number $\left(\frac{g\beta\Delta(T_H-T_C)L^3}{\nu^2}\right)$
Ri	Richardson number
P	dimensionless pressure
p	pressure (N m^{-2})
T	temperature (K)
θ	dimensionless temperature
t	time (s)
x, y	Cartesian coordinates (m)
X, Y	dimensionless Cartesian coordinates
u, v	components of velocity in x and y directions (m/s)
U, V	dimensionless of velocity components in X and Y directions
L	width of cavity (m)
V_l	left wall velocity
V_r	right wall velocity
Nu	Nusselt number
Nu_m	average Nusselt number
V_r	right wall velocity

Greek letters

τ	dimensionless time
ψ	stream function
α	thermal diffusivity ($k/(\rho C_p)$) (m^2/s)
β	coefficient of volume expansion (K^{-1})
ϕ	solid volume fraction
μ	dynamic viscosity (Pa s)
ρ	density (kg/m^3)

Subscripts

f	fluid
m	average
nf	nanofluid
o	reference state
s	solid
C	cold
H	hot

sided lid-driven differentially heated square cavity filled with copper–water nanofluid. They observed that the average Nusselt number increased substantially with the increase of the volume fraction of the nanoparticles, for a fixed Richardson number. The effect of nanoparticle concentration and the viscosity effects are found experimentally by Nguyen et al. [6] and Angue Minsta et al. [7] for various temperature values. It is found that on increment of concentration of the nanoparticles, the viscosity and temperature decrease sharply. Recently, Selimefendigil and Oztop [13] studied natural convection of nanofluid flow with different shaped obstacles including diamond, square and circular and discussed the affect of solid volume fraction and obstacle shapes on thermal patterns. In another study, Selimefendigil et al. [14] investigated the heat transfer and fluid flow in the presence of magnetic dipole in a partially heated cavity. They observed that the averaged heat transfer along the heat source is found to be minimum when magnetic dipole source is placed at the middle of the vertical wall.

Muthtamilselvan et al. [8] numerically investigated the mixed convection and heat transfer in a lid-driven enclosure filled with copper–water nanofluid, and observed that the heat transfer has a large effect on solid volume fraction and aspect ratio of the enclosure. Abu-Nada et al. [9] studied the heat transfer effect in a differentially heated enclosure using variable properties of CuO–water and Al_2O_3–water nanofluids due to natural convection. They found that for high Rayleigh number variation of average heat transfer is less sensitive in the case of thermal conductivity model than that of the viscosity model. Abbasian et al. [10] numerically studied the mixed convection with Cu–water nanofluid in a lid-driven cavity, where the horizontal walls are kept insulated and vertical walls are heated sinusoidally. They observed that with a decrease of Richardson number and an increase of volume fraction of nanoparticles there is an increase of heat transfer. Also, it is found that for a constant Reynolds number, the rate of heat transfer increases with the increase of Richardson number. Talebi et al. [11] numerically studied the problem of mixed convection flow of copper–water nanofluid in a lid-driven cavity with differentially heated vertical walls and shown the increment of average Nusselt number with the solid volume fraction over constant Reynolds and Rayleigh numbers. Mahmoudi et al. [12] studied the problem of mixed convection in a vented square cavity filled with copperwater nanofluid. It is observed that for higher Reynolds and Richardson number the presence of nanoparticles have more effect on increasing the heat transfer performance. A extensive study of mixed convection has been conducted by Selimefendigil et al. [15–23] for various geometries.

A finite volume approach is used by Sebdani et al. [25] to investigate the fluid flow and heat transfer in a square cavity filled with Al_2O_3–water nanofluid with a bottom wall heated source. Both the vertical walls of the cavity are maintained at cold temperature and moving downward with constant velocity whereas the horizontal walls are taken to be adiabatic and fixed. On addition of nanoparticles it is observed that heat transfer effect is enhanced with increase of Reynolds number, for a fixed Rayleigh number. Garoosi et al. [26,27] applied finite volume approach based on SIMPLE algorithm for simulation of mixed convection of nanofluid and concluded that at low Richardson number the nanoparticle distribution remains almost uniform. Moumni et al. [31] studied the heat transfer characteristics of various water-based nanofluids in a two-sided square lid driven cavity, using a pair of discrete heat sources with different locations at the bottom wall of the cavity. The heat transfer rate increases with an increase in Reynolds number, Richardson number and solid volume fraction, and rate of heat transfer increment is found to be higher in the case of Cu–water and Ag–water nanofluids as compared to Al_2O_3–water and TiO_2–water nanofluids.

Generally, two approaches are employed for the numerical study of the velocity field, heat transfer and temperature distribution in nanofluids namely; single phase and two phase models. In the former approach, it is assumed that the nanoparticles and the continuum phase are in thermal equilibrium and have the same velocity. Many researchers oppose the validity of single phase models as the slip velocity between the base fluid and nanoparticles may not be zero. Therefore, they encouraged the two phase model which is a more complex approach. For nanoparticles having higher thermal conductivity such as Cu ($K = 400$) which have also been used in the present study, Garoosi et al. [24,32] validated the use of a single-phase model, showing that for the nanoparticles with higher thermal conductivity the thermophoretic effect is negligible. Moreover, in another study Garoosi et al. [33] stated that for a low Richardson number the effect of drag, gravity and buoyancy

forces on nanoparticle distribution is negligible, which again validates the use of a single phase model in the present study. Recently, Garoosi et al. [34,35] used the single phase method for the simulation of nanoparticles.

Based on the above studies it is found that there is lack of studies for the complete heat transfer effects based on mixed convection for differentially heated horizontal walls with moving vertical walls. It is also observed [36] that the heat transfer effects are mostly influenced by the movement of walls. The heat transfer rate is less when vertical walls are moving upward in comparison to the movement which is in the opposite direction. The present study deals with the comparative study of mixed convection flow of Cu–water based nanofluid in a two-sided lid-driven cavity. Both the horizontal walls are kept fixed and the vertical walls are moving. Four different cases of study have been made on the basis of direction of moving walls with a fixed location of two discrete heat sources on the bottom walls, keeping the other walls at lower temperature. The effective thermal conductivity and the viscosity of the nanofluids are determined using Maxwell model [28] and Brinkman model [29] respectively. The effect of various flow governing parameters (Re, Ri, ϕ) with a fixed value of Prandtl number ($Pr = 6.2$) on the flow and heat transfer has been investigated. Heat transfer enhancement is analyzed based on different physical parameters.

2. Problem definition and mathematical modeling

In the present study two sided lid-driven square cavity of length L, filled with nanofluid is considered as shown in Fig. 1. Two equal portions of length $L/4$ of lower walls are maintained at a higher temperature T_H and rest of the bottom wall is kept insulated. All other walls are maintained at relatively lower temperature (T_C). We have considered four cases: In Case I, left vertical wall is moving upward and the right one is moving downward. In Case II, the left wall is moving downward and the right one is moving upward. In Case-III, both the vertical walls are moving downward and in Case IV both the walls are moving upward.

The nanofluid flow is assumed to be steady, laminar, and the fluid is assumed to be Newtonian, incompressible and is in thermal equilibrium with no slip condition between two phases. Except density, the thermophysical properties of the nanofluid are assumed to be constant. The density variation is based on Boussinesq approximation. Further, the shape and size of the nanoparticles are assumed to be uniform. The thermophysical properties of water and copper at the reference temperature are presented in Table 1 [12].

The governing equations for a unsteady, two-dimensional laminar and incompressible flow are expressed as:

$$\frac{\partial u}{\partial x}+\frac{\partial v}{\partial y}=0, \tag{1}$$

Table 1
Thermophysical properties of water and copper.

Property	Water	Copper
C_p	4179	383
ρ	997.1	8954
k	0.6	400
β	2.1×10^{-4}	1.67×10^{-5}

$$\frac{\partial u}{\partial t}+\frac{\partial (uu)}{\partial x}+\frac{\partial (uv)}{\partial y}=-\frac{1}{\rho_{nf}}\frac{\partial p}{\partial x}+\frac{\mu_{nf}}{\rho_{nf}}\left(\frac{\partial^2 u}{\partial x^2}+\frac{\partial^2 u}{\partial y^2}\right), \tag{2}$$

$$\frac{\partial v}{\partial t}+\frac{\partial (uv)}{\partial x}+\frac{\partial (vv)}{\partial y}=-\frac{1}{\rho_{nf}}\frac{\partial p}{\partial y}+\frac{\mu_{nf}}{\rho_{nf}}\left(\frac{\partial^2 v}{\partial x^2}+\frac{\partial^2 v}{\partial y^2}\right)+\frac{(\rho\beta)_{nf}}{\rho_{nf}}g(T-T_c),$$

$$\frac{\partial T}{\partial t}+\frac{\partial (uT)}{\partial x}+\frac{\partial (vT)}{\partial y}=\alpha_{nf}\left(\frac{\partial^2 T}{\partial x^2}+\frac{\partial^2 T}{\partial y^2}\right) \tag{3}$$

where, the thermal diffusivity α_{nf}, the effective density of nanofluid at reference temperature ρ_{nf} and the heat capacitance of nanofluid $(\rho C_p)_{nf}$ are given as [10],

$$\alpha_{nf}=k_{nf}/(\rho C_p)_{nf}, \tag{4}$$

$$\rho_{nf}=(1-\phi)\rho_f+\phi\rho_s, \tag{5}$$

$$(\rho C_p)_{nf}=(1-\phi)(\rho C_p)_f+\phi(\rho C_p)_s, \tag{6}$$

$$(\rho\beta)_{nf}=(1-\phi)(\rho\beta)_f+\phi(\rho\beta)_s. \tag{7}$$

where, $\rho_{nf}, \rho_f, \rho_s$ and ϕ are the density of nanofluid, density of base fluid, density of nanoparticle and volume fraction of the nanoparticles, respectively.

The effective thermal conductivity of the nanofluid is approximated by the Maxwell self-consistent approximation model. For the two-component entity of spherical-particle suspension, the Maxwell model [28] gives,

$$\frac{k_{nf}}{k_f}=\frac{k_s+2k_f-2\phi(k_f-k_s)}{k_s+2k_f+\phi(k_f-k_s)}. \tag{8}$$

The effective viscosity of nanofluid is given by Brinkmann [29] as follows,

$$\mu_{nf}=\frac{\mu_f}{(1-\phi)^{2.5}}. \tag{9}$$

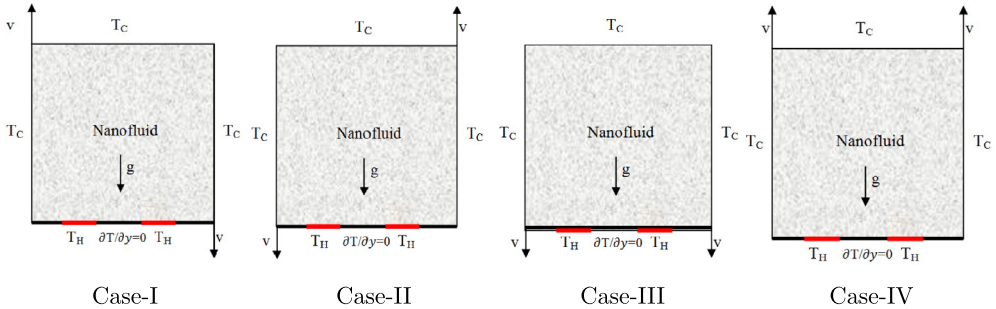

Fig. 1. Problem geometry.

The given formulation of the effective thermal conductivity and effective viscosity is found to be appropriate by various authors [5,8–10,31].

The above mentioned equations can be expressed in non-dimensional form by incorporating the following dimensionless variables,

$$X=\frac{x}{L};\quad Y=\frac{y}{L};\quad U=\frac{u}{U_0};\quad V=\frac{v}{U_0};\quad \theta=\frac{T-T_C}{T_H-T_C};$$
$$\tau=\frac{tU_0}{L};\quad P=\frac{p}{\rho_{nf}U_0^2};\quad Re=\frac{U_0L}{\nu_f};\quad Pr=\frac{\nu_f}{\alpha_f};\quad Ri=\frac{g\beta L(T_H-T_C)}{U_0^2}. \tag{10}$$

The governing equations in dimensionless form by considering the above mentioned assumptions can be rewritten as,

$$\frac{\partial U}{\partial X}+\frac{\partial V}{\partial Y}=0, \tag{11}$$

$$\frac{\partial U}{\partial \tau}+\frac{\partial (UU)}{\partial X}+\frac{\partial (UV)}{\partial Y}=-\frac{\partial P}{\partial X}+\frac{1}{Re}\frac{\rho_f}{\rho_{nf}}\frac{1}{(1-\phi)^{2.5}}\left(\frac{\partial^2 U}{\partial X^2}+\frac{\partial^2 U}{\partial Y^2}\right), \tag{12}$$

$$\frac{\partial V}{\partial \tau}+\frac{\partial (UV)}{\partial X}+\frac{\partial (VV)}{\partial Y}=-\frac{\partial P}{\partial Y}+\frac{1}{Re}\frac{\rho_f}{\rho_{nf}}\frac{1}{(1-\phi)^{2.5}}\left(\frac{\partial^2 V}{\partial X^2}+\frac{\partial^2 V}{\partial Y^2}\right)+Ri\frac{\rho_f}{\rho_{nf}}\left(1-\phi+\phi\frac{\rho_s\beta_s}{\rho_f\beta_f}\right)\theta,$$

$$\frac{\partial \theta}{\partial \tau}+\frac{\partial U\theta}{\partial x}+\frac{\partial V\theta}{\partial y}=\frac{1}{RePr}\frac{k_{nf}}{k_f}\frac{(\rho C_p)_f}{(\rho C_p)_{nf}}\left(\frac{\partial^2\theta}{\partial x^2}+\frac{\partial^2\theta}{\partial y^2}\right). \tag{13}$$

The relevant boundary conditions are given by,

$$U=0,\ V=V_l,\ \theta=0\quad \text{if}\quad X=0,\quad Y\in[0,1]; \tag{14}$$

$$U=0,\ V=V_r,\ \theta=0\quad \text{if}\quad X=1,\quad Y\in[0,1]; \tag{15}$$

$$U=V=0,\begin{cases}\theta=1 & \text{if } X\in(1/8,3/8]\cup(5/8,7/8]\\ \frac{\partial\theta}{\partial Y}=0 & \text{elsewhere}\end{cases},Y=0$$

$$U=0,\ V=0,\ \theta=0\quad \text{if}\quad X\in[0,1],\quad Y=1. \tag{16}$$

Four different cases are discussed according to boundary conditions on the left and right wall given by,

Case I: $V_l=1$, $V_r=-1$,
Case II: $V_l=-1$, $V_r=1$,
Case III: $V_l=1$, $V_r=1$,
Case IV: $V_l=-1$, $V_r=-1$.

In order to calculate the heat transfer enhancement, we have calculated Nu (Nusselt number) and Nu_m (average Nusselt number) along the heated surfaces as,

$$Nu(X)=-\frac{k_{nf}}{k_f}\left(\frac{\partial\theta}{\partial X}\right)_{hot\ wall}, \tag{17}$$

$$Nu_{m_i}=\frac{\int_{hot\ wall}Nu(X)dX}{\int_{hot\ wall}dX}. \tag{18}$$

The overall surface average Nusselt number is the average of $Nu_{m_{s_1}}$ and $Nu_{m_{s_2}}$.

3. Numerical procedure

A finite volume approach [30] is used to solve the set of governing equations using the staggered grid algorithm with uniform grid arrangement. Semi-implicit method for pressure linked equations (SIMPLE) is used to couple the continuity equation with Navier–Stokes equations in their discretized form. To solve the discretized system of momentum and energy equations we used the Thomas algorithm (TDMA). When flows are dominated by convection effects then the numerical instability will be achieved for higher Reynolds number. The implicit scheme is used for time steps. In order to linearize the nonlinear system of partial differential equations, a quasi-linearization approximation has been employed.

At every time step, we approximate the nonlinear term as

$$\left(u\frac{\partial u}{\partial x}\right)^{n+1}=u^n\left(\frac{\partial u}{\partial x}\right)^{n+1}, \tag{19}$$

with $n\geqslant 0$, is the iteration index. The convective terms are discretized by third-order accurate upwind difference scheme given by

$$u_{ij}\left(\frac{\partial u}{\partial x}\right)=u_{ij}(u_{i+2j}-2u_{i+1j}+9u_{ij}-10u_{i-1j}+2u_{i-2j})/(6\delta x) \tag{20}$$

for u_{ij} positive and,

$$u_{ij}\left(\frac{\partial u}{\partial x}\right)=u_{ij}(-2u_{i+2j}+10u_{i+1j}-9u_{ij}+2u_{i-1j}-u_{i-2j})/(6\delta x) \tag{21}$$

for u_{ij} negative.

The truncation error of this scheme is given by

$$\frac{1}{4}(\delta x)^3\left(u_{ij}\frac{\partial^4 u}{\partial x^4}\right). \tag{22}$$

The expression for u, near the wall is obtained by a second order central difference scheme as,

$$u_{ij}\left(\frac{\partial u}{\partial x}\right)=u_{ij}(u_{i+1j}-u_{i-1j})/(2\delta x)+O(\delta x^2). \tag{23}$$

The diffusion terms are discretized through a second-order accurate central-difference scheme, which is conducive to a stable solution as,

$$(u_{xx})_{ij}=(u_{i-1j}-2u_{ij}+u_{i+1j})/(\delta x)^2,$$

$$(u_{yy})_{ij}=(u_{ij-1}-2u_{ij}+u_{ij+1})/(\delta y)^2.$$

The second order Poisson equation is discretized through a upwind spatial difference scheme. The resulting algebraic equations are solved using the successive over relaxation (SOR) method. SOR method is used to combat the non-linear nature of governing equations. The convergence criterion used throughout the calculation velocities, temperature and pressure correction is defined by the expression,

$$\epsilon=\left|\tau_{i,j}^{n+1}-\tau_{i,j}^{n}\right|\leqslant 10^{-5} \tag{24}$$

where, ϵ is the tolerance in any time level and τ represents the flow variables.

4. Grid independency test and code validation

A grid independency test is performed for grid sizes varying from 61×61 to 121×121. A comparison of grid size effect is made with Muthtamilselvan et al. [8] and is presented in Fig. 2(a). A lid driven cavity filled with nanofluid is considered in which the upper lid is maintained at high temperature, lower lid with low temperature and all other walls are kept adiabatic. The results for vertical

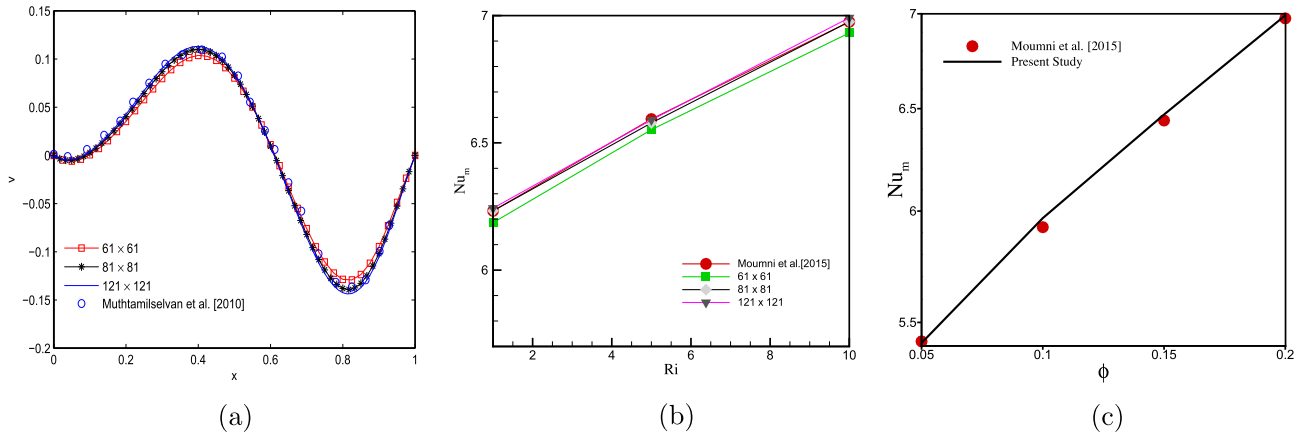

Fig. 2. Comparison of (a) vertical component of velocity at mid section of cavity due to Muthtamilselvan et al. [8] for $Ri = 1, Ra = 100, \phi = 2\%$, for various grid size from 61×61 to 121×121, (b) average Nusselt number with results due to [31] with $Pr = 6.2, \phi = 2\%, Re = 100$ and $1 \leqslant Ri \leqslant 10$ for various grid size from 61×61 to 121×121, (c) average Nusselt number with results due to [31] with $Pr = 6.2, Ri = 10, Re = 100$ and $0.05 \leqslant \phi \leqslant 0.2$.

v-velocity are compared for $Ri = 1, Ra = 100$ and $\phi = 2\%$ and for grid size 81×81, our results are found to be optimum and in good agreement with results due to Muthtamilselvan et al. [8]. Another grid independency test is performed for grid sizes varying from 61×61 to 121×121. A average Nusselt number comparison of grid size effect is made with Moumni et al. [31] with $Pr = 6.2, \phi = 2\%, Re = 100$ and $1 \leqslant Ri \leqslant 10$ and is presented in Fig. 2(b). Our results for grid size 81×81 are found to be optimum and in good agreement with results due to Moumni et al. [31]. Hence, the grid size 81×81 is chosen for all of further computations. A comparison of average Nusselt number for different solid volume fraction is made with Moumni et al. [31]. A mixed convection flow with Cu–water nanofluid is considered in a two-sided lid-driven square cavity . Fig. 2(c) shows the variation of average Nusselt number with different solid volume fractions for $Ri = 10, Re = 100$ and $\phi = 0.2$. The maximum percentage difference of average Nusselt number from the result due to Moumni et al. [31] is 0.7%.

5. Results and discussion

Mixed convection in a two sided lid-driven cavity filled with Cu–water nanofluid is examined for the heat transfer effect, in which two discrete heat sources of length $L/4$ are placed at the bottom wall at a distance $L/8$ and $7L/8$ from the left wall respectively. The flow governing parameters are Richardson number, Rayleigh number and solid volume fraction ratio and the ranges are $0.1 \leqslant Ri \leqslant 10, 1 \leqslant Re \leqslant 100, 0 \leqslant \phi \leqslant 0.2$. Four different configurations are chosen based on the direction of moving lids. In the figures of streamlines, dashed lines show the clockwise direction (i.e. negative stream function values) of fluid flow whereas the plain lines show the anticlockwise direction (i.e. positive stream function values) of fluid flow in the streamline plots.

Case-I: In Case-I, the left lid is moving upward and the right lid is moving downward. Figs. 3 and 4 represent the streamlines (left) and isotherms (right) for $Ri = 0.1, 10$ with $1 \leqslant Re \leqslant 100$ and $\phi = 0.2$. It is found that due to heat source strength along the lower boundary the flow is symmetric along vertical mid-line for low Reynolds number ($Re = 1$, Figs. 3(a) and 4(a)) and it is dominated by natural convection. A conductive regime is formed with two inner cells at the center of the cavity. But with increase in Reynolds number, the forced convection comes into effect and the fluid starts moving upward from the left and downward from the right side (Figs. 3(c,e) and 4(c,e)). The effect can be easily seen at the core of the cavity where the eddy is no more horizontal as observed for $Re = 1$. As the Reynolds number increases, the flow develops a convective cell and tiny inner cells vanishes as the flow is dominated by forced convection. As Richardson number increases with $\phi = 0.2$, the eddy size increases due to buoyancy effect as observed in Fig. 4(a). From Figs. 3(b) and 4(b), it is observed that small clockwise rotating hot cells appear close to the bottom heating location and isotherms are parallel to the heat sources. The uniform distribution of the isotherm indicates the conduction mode of heat transfer and represents a hyperbolic pattern. As Reynolds number increases, the clockwise rotating cells grow in size, move away from the boundary layer and forced convection dominates the heat transfer effect. Due to the movement of lids the cold fluid moves toward the right wall and hot fluid is confined to the boundary layer entrained to the whole cavity.

From Figs. 3(c,e) and 4(c,e), it can be observed that the vortex length gets stronger as Reynolds number increases. The values of flow lines increases up to 1.6% for Reynolds number varying from 50 to 100 as observed from Fig. 3(c) and (d) for a fixed value of Richardson number and solid volume fraction. The flow is completely dominated by forced convection rather than natural convection.

The heat transfer changes its pattern at higher Reynolds number. The cold fluid adjacent to left vertical wall moves toward the top wall and return to the core section of the cavity due to the frictional effect of the right moving wall. As Reynolds number increases from 50 to 100, cold fluid remains centered at the middle of the cavity and the heat transfer lines are more circular as observed in Fig. 3(f) compared to Fig. 3(d) where the isothermal lines are parallel to the top wall. The heat transfer effect due to forced convection is more significant as compared to the natural driven effect. Similar effect of heat and flow transfer is also observed as Richardson number is increasing from 0.1 to 10 for higher Reynolds number.

As Richardson number increases for 0.1–10 for $Re = 50$ the vortex along the core tilted downward and gets stronger as compared to $Ri = 0.1$. The flow strength is increasing up to 2.7% as observed from Figs. 3(c) and 4(c). This signifies that buoyancy driven flow is more effective than forced and natural convection effects.

Case-II: In this case left side wall is moving downward while the right wall is moving upward which represents aiding shear and buoyancy effects. Figs. 5 and 6 represents streamlines and isotherms for $Ri = 0.1$ and $Ri = 10$ and are observed to be the same profile as obtained in earlier case but the circulation pattern changes from anticlockwise to clockwise direction due to the movement of lids in the opposite direction. For the validation if

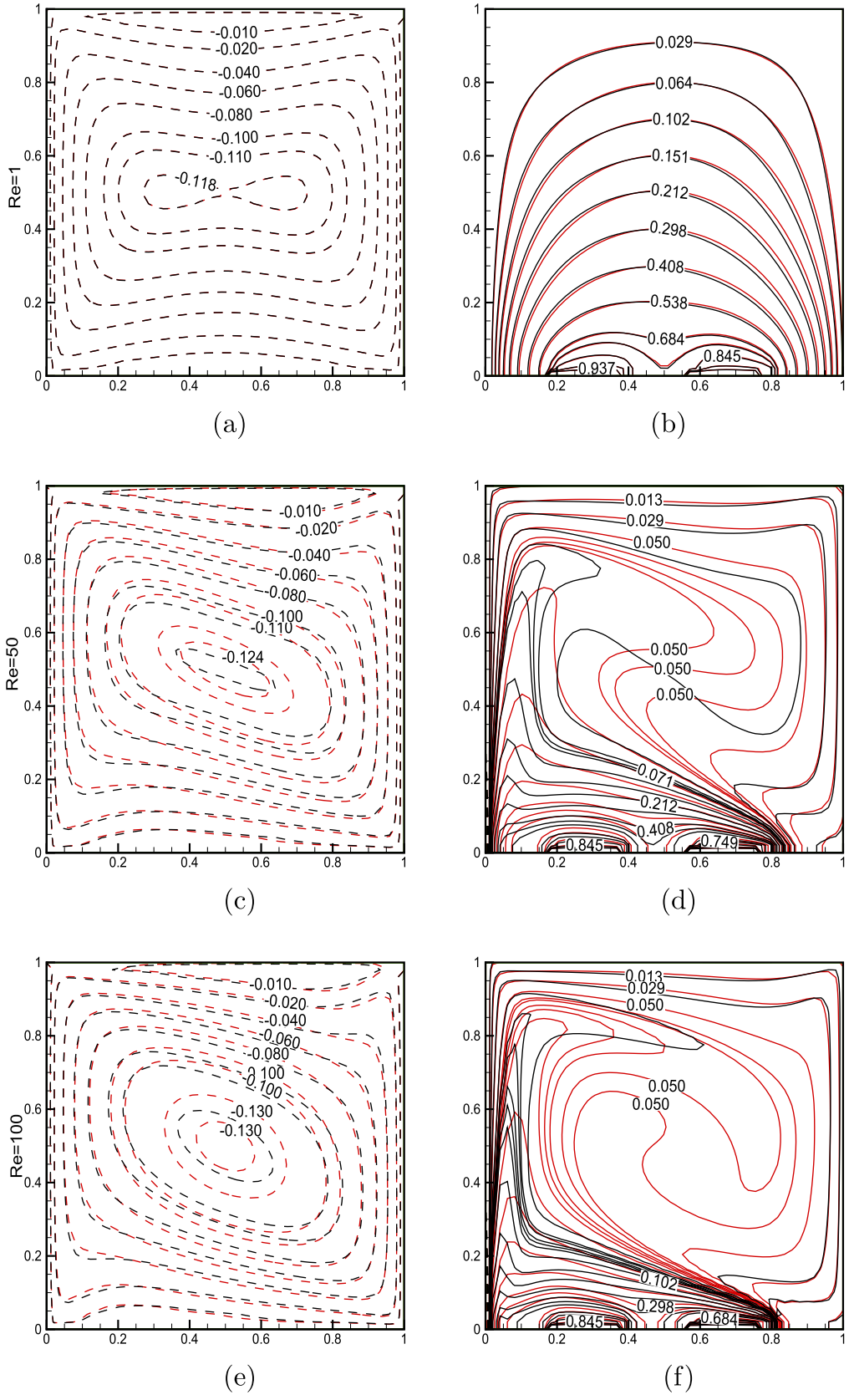

Fig. 3. Streamlines and isotherm lines of clear fluid ($\phi = 0.0$, Black) and nanofluid ($\phi = 0.2$, Red) at $Ri = 0.1$, $1 \leqslant Re \leqslant 100$ for Case-I.

we are comparing the result obtained by Oztop and Dagtekin [36] for a clear fluid case it can be found that our result has a very good agreement with them. For Fig. 5(c,e) it can be observed that the vortex strength remains the same but the vortex is tilted down toward the left vertical wall and the cell center moves toward the left vertical wall due to the forced convection. From Fig. 5(c)

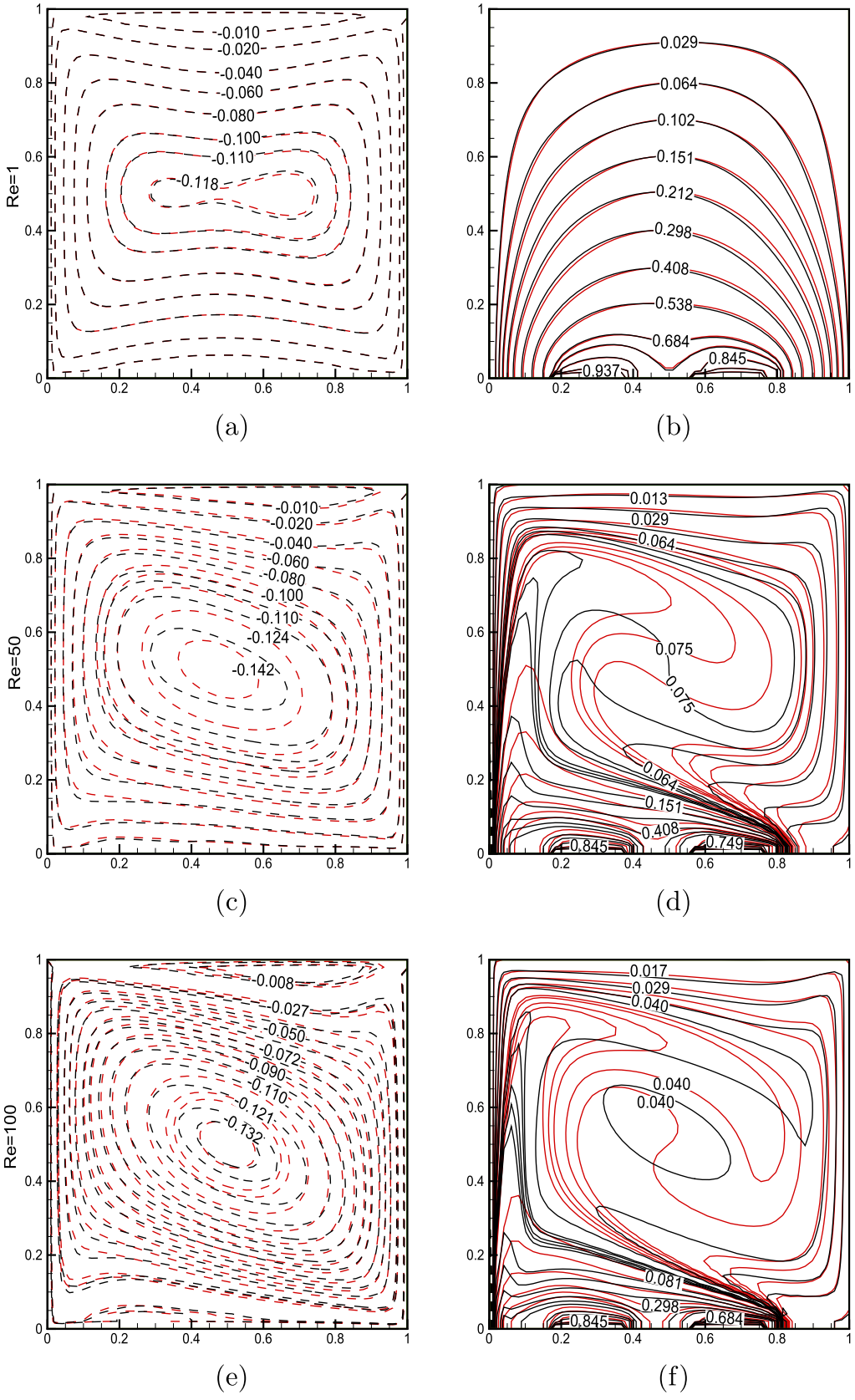

Fig. 4. Streamlines and isotherm lines of clear fluid ($\phi = 0.0$, Black) and nanofluid ($\phi = 0.2$, Red) at $Ri = 10$, $1 \leqslant Re \leqslant 100$ for Case-I.

it is observed that $|\psi_{centre}| = 0.129$ at $x = 5.62$ and $y = 5.1$ and from Fig. 6(c) $|\psi_{centre}| = 0.162$ at $x = 5.2$ and $y = 4.5$. From Figs. 5(c,e) and 6(c,e) it is observed that for higher Reynolds number the stream function values increases. On increasing Ri values from 0.1 to 10 an increment of 25% and 21.02% in stream function values is observed for $Re = 50$ and $Re = 100$ respectively.

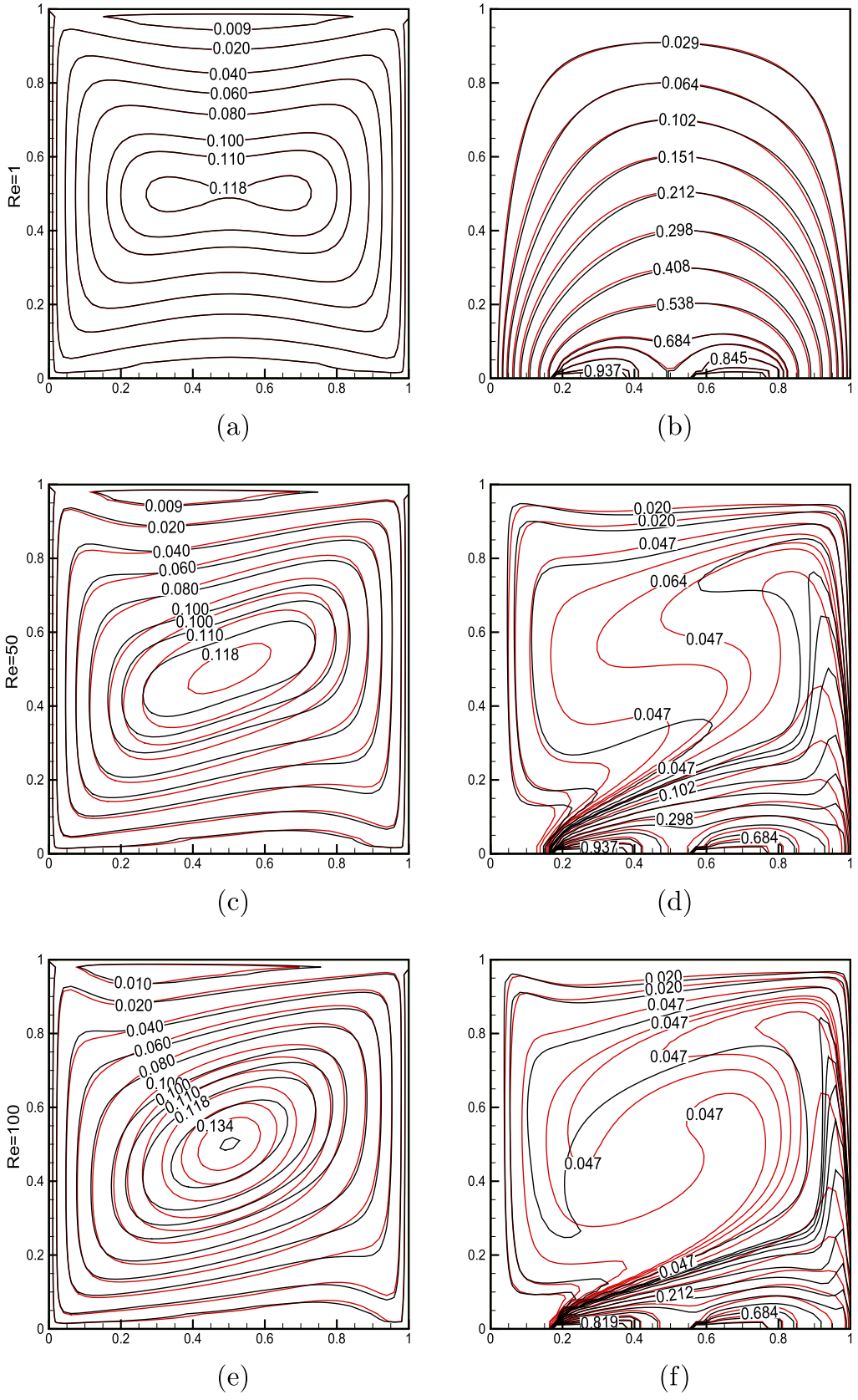

Fig. 5. Streamlines and isotherm lines of clear fluid ($\phi = 0.0$, Black) and nanofluid ($\phi = 0.2$, Red) at $Ri = 0.1$, $1 \leqslant Re \leqslant 100$ for Case-II.

The flow pattern of isothermal lines are completely opposite at the higher Reynolds number (Fig. 5(d,f)). At $Re = 1$ the flow pattern and isotherms are unaltered but the energy transfer in the central region is not much altered. From Fig. 6 it can be observed that variation of Ri does not affect much compared to earlier case. For higher Reynolds number the stream function values (Fig. 6(c,e))

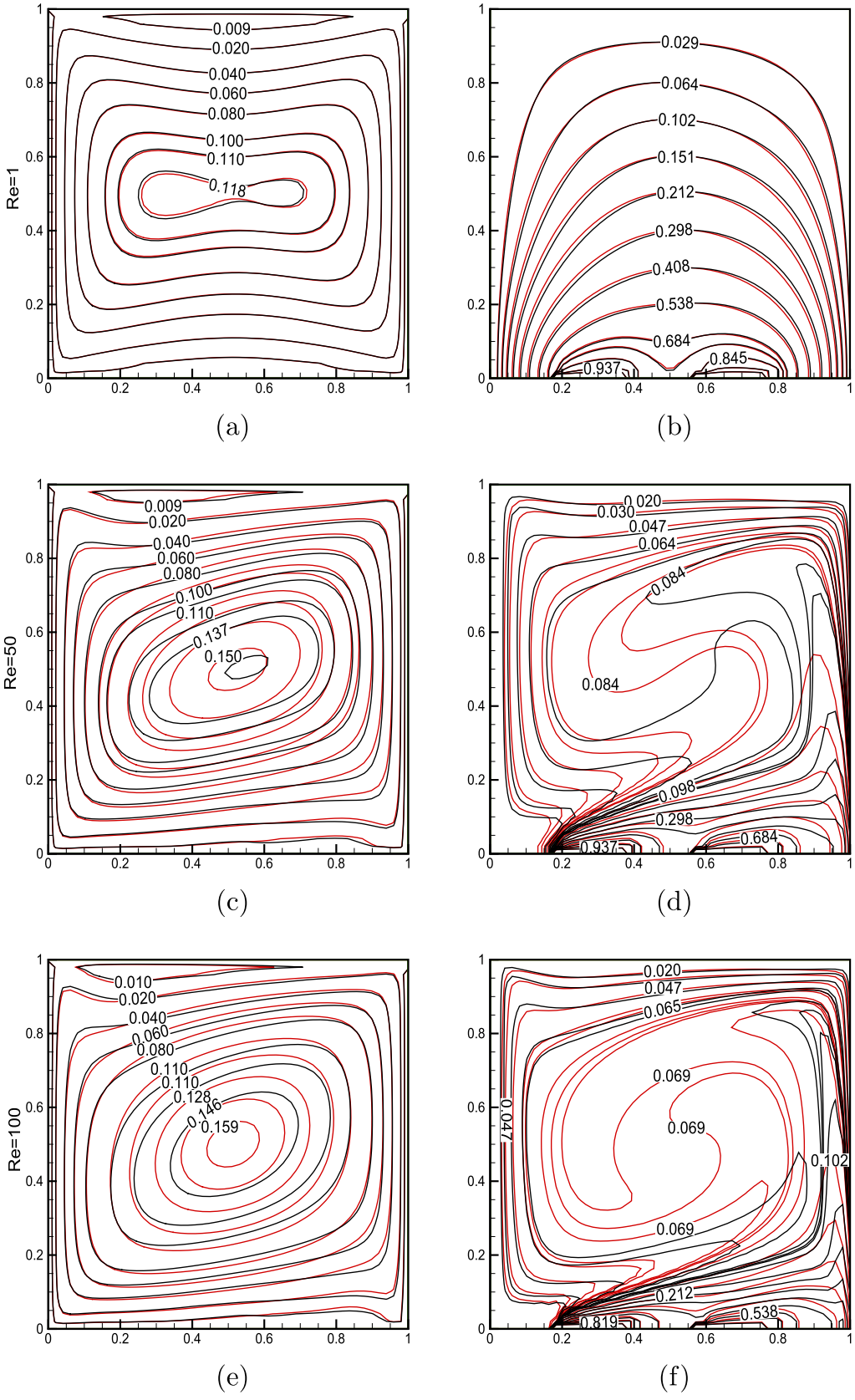

Fig. 6. Streamlines and isotherm lines of clear fluid ($\phi = 0.0$, Black) and nanofluid ($\phi = 0.2$, Red) at $Ri = 10$, $1 \leqslant Re \leqslant 100$ for Case-II.

are increasing toward the cell center of the cavity due to strong buoyancy driven effect.

Case-III: In this case, both the vertical walls move downward in which the shear force is supported by the buoyancy effects. Figs. 7 and 8 represent the streamlines (left) and isotherms (right) for $Ri = 0.1$ and $Ri = 10$ respectively with the variation of Reynolds number from $1 \leqslant Re \leqslant 100$. The streamline profiles Fig. 7(a,c,e) shows the development of Rayleigh–Benard convection cell above each heat source. Also with the increase in the Richardson number from $Ri = 0.1$ to 10 the stream function value increases by 23.56% in the core of the cavity for higher Reynolds number ($Re = 100$) which shows the buoyancy dominated effect on shear effect. The temperature profiles (7(b,d,f)) shows heat plums developed above each heat source. Buoyancy forces drive the heated fluid toward the upper cold surface from the heat source and upper cold fluid move downward. The temperature of cold fluid again rises due to the heat source and move upward which repeats the flow pattern. The closest layer of fluid makes a stable recirculation zone centered along the edges of each heat source. In this case it is clearly observed that buoyancy forces are supporting the shear forces. From Fig. 7(b) the heat transfer lines parallel to the heat sources but as Reynolds number increases, the lids drag the cold fluid toward the hot surface forming a sharp paraboloid profile. This signifies that hot fluid passes toward the center and upper cold region of the cavity only in the middle section where the shear effect is minimum.

From Fig. 8, similar configurations for streamlines are observed for higher buoyancy forces $Ri = 10$. The flow profiles show two anticlockwise vortices as observed in case of Fig. 7 but the strong vortices signifies the larger velocity values. From Fig. 8(a,c,e) it is observed that flow velocity is increasing as Reynolds number is increasing but stagnant flow is observed at $Re = 50$ and $Re = 100$.

The heat transfer effect is found to be significant at higher Reynolds number for $Re = 100$ (Fig. 8(f)). At higher Reynolds number $Re = 50$ and $Re = 100$ (Fig. 8(d,f)) it is found that shear force is dominating the heat transfer effect and most of the cold fluid tries to store close to the lower left and right corner of the cavity. The heat transfer rate is found to be less as Re increases. The central heat transfer value at $Re = 50$ is 0.335 at (0.5, 0.42) but this moves to the position (0.5, 0.34) for $Re = 100$.

Case-IV: Streamlines and isotherm lines for Case-IV is presented in Figs. 9 and 10. In this case two vertical parallel lids are moving in the upward direction in which shear effect is opposed by the buoyancy driven flow. Since two lids are moving in the same direction and effective velocities are influenced by the buoyancy effects. From 9(a,c,e) it is observed that for $Ri = 0.1$ as Re is increasing the fluid circulated vortices are moving upward supporting the shear effect as compared to buoyancy effects and magnitude of velocities are decreasing as compare to earlier case. An increment of 7.21% in stream function value at the center of the eddy is observed for $Re = 100$ on increasing Ri values from 0.1 to 10. The heat transfer lines presented in Fig. 9(b,d,f), shows that at low Reynolds number the flow is dominated by buoyancy effect and found to be similar profile as obtained in earlier case. But as Re increases the flow is dominated by forced convection effect and buoyancy has minimal effect. The cold fluid parallel to the moving boundaries forced to move to the core region of cavity and heated fluid moves toward the moving boundaries to fill the portion. Hence heat transfer is minimized at higher Reynolds number. The flow is completely forced dominated at larger Reynolds number. From Fig. 9(d,f) it is found that the heat transfer values in the core is reduced from 0.0060 at (0.5, 0.4) to 0.0055 at (0.5, 0.4). Fig. 10 represents the flow and isothermal lines for $Ri = 10$, where similar flow profiles are obtained as observed in Fig. 9. These figures are mirror images of earlier Case-III but the flow circulation are reversed in order due to the opposing shear effect. Streamlines are symmetric about the right and left half of the cavity which is also same for Case-III but the orientation is opposite. From Fig. 10(a,c,e) it is observed that vortex strength is increased with increase of Reynolds number but shifts upward.

The heat transfer lines presented in Fig. 10(d,f) heat transfer rate is increasing due to the increase of Ri values. From Fig. 10(d,f) it is found that cold fluid forces to enter near to heat source for higher Reynolds number. For the higher Reynolds number as Ri is increased the isotherms are clustered close to the sliding wall and forming vortices along the upper section of the enclosure.

Overall flow and heat transfer: The flow and heat transfer in all the four different considered configurations are found to be natural convection dominated regimes when $Ri = 10$ and forced convection dominated regimes when $Ri = 0.1$. The increment of Re shows the dominating effect of forced convection over natural convection. For Case-I and Case-II the flow and heat transfer are identical irrespective of the variation of Ri. The isotherm plot shows that heat transfer is mostly carried out by the moving lids in upward direction, the heated fluid is transported to the colder part and cold fluid comes down along the downward moving lid. In Case-III and Case-IV we can observe that heat transfer is reduced in comparison to Case-I and Case-II. This signifies that heat transfer is increasing when the lids are moving in opposite direction. In all the four cases it is found that heat transfer lines are almost similar for $Re = 1$. This signifies that heat transfer is almost constant in lower Reynolds number for different Ri values and also independent of the direction of moving lids. In the final form, the average Nusselt number for four cases and different solid volume fraction are calculated and presented in Fig. 11 using Eq. (18). From Fig. 11(i), it is observed that the heat transfer efficiency is increasing with the increment of solid volume fraction value ϕ. A sudden variation of average Nusselt number is observed when Re is increased from 1 to 50 and 50 to 100. It is observed that average heat transfer at $Re = 50$ with high nanofluid concentration is higher than at $Re = 100$ with clear fluid. This implies that nanoparticles are very much responsible and capable to change the flow features. For Case-II, Case-III and Case-IV the average Nusselt number represented by Fig. 11(ii,iii,iv) shows that average Nusselt number is increasing with Richardson number and solid volume fraction.

For all the cases it is observed that average Nusselt number is almost constant at $Re = 1$ for all the Richardson number but with increase in Re the variation due to Richardson number is clearly visible except in Case-IV at $Re = 10$. The Nusselt number is found to be increasing for all values of Richardson number and Reynolds number with solid volume fraction.

From the above observations we can conclude that average Nusselt number along the cavity floor is found to be highest in Case-II in comparison to all other considered cases for all Ri and ϕ values. Increment of solid volume fraction increases the heat transfer rate of nanofluid very efficiently. In Case-I, heat transfer rate increment is found to be 47.52% with $Ri = 0.1$ and 45.8% with $Ri = 10$ for $Re = 100$ in Cu–water nanofluid where the solid volume fraction is changing from 0.0% to 20%. Similarly in Case-II the variation is found to be 47.73% for $Ri = 0.1$ and 40.65% for $Ri = 10$, in Case-III it is about 49.82% for $Ri = 0.1$ and 39.12% for $Ri = 10$ and in Case-IV, the variation is 44.07% and 30.39% for $Ri = 0.1$ and 10 respectively. The maximum value of average Nusselt number in Case-I to IV are found to be 4.5308, 7.7599, 6.9914 and 6.1112 respectively at $Ri = 10$, $Re = 100$ and $\phi = 0.2$. Hence, the solid volume fraction is found to be most effective in Case-I as the increment in average Nusselt number is found to be best for all Ri but still the overall heat transfer is minimum in this case as the average Nusselt number values are minimum as compared to other cases. The maximum heat transfer is obtained in Case-II, as the average Nusselt number values for all parameters are maximum in this case.

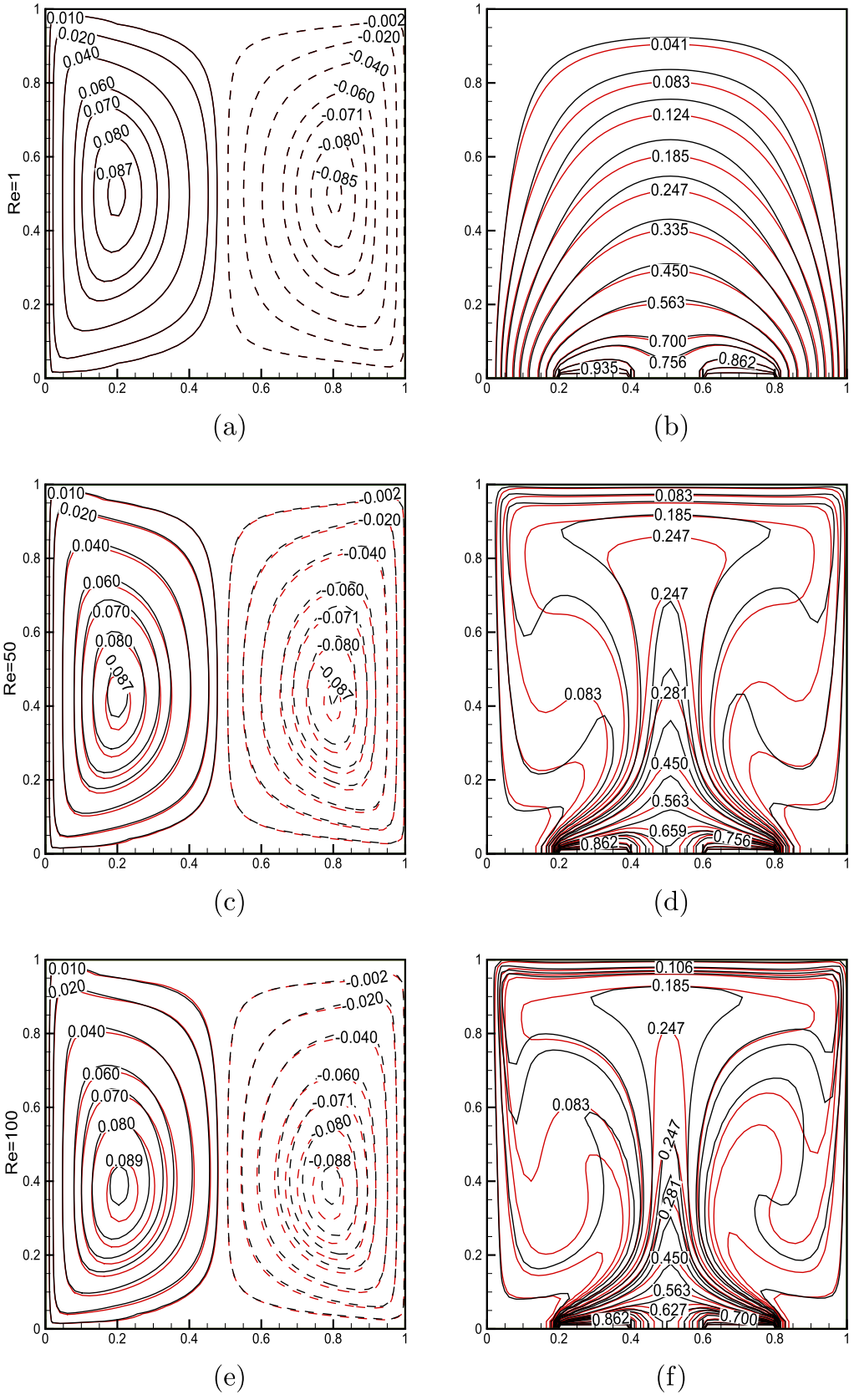

Fig. 7. Streamlines and isotherm lines of clear fluid ($\phi = 0.0$, Black) and nanofluid ($\phi = 0.2$, Red) at $Ri = 0.1$, $1 \leqslant Re \leqslant 100$ for Case-III.

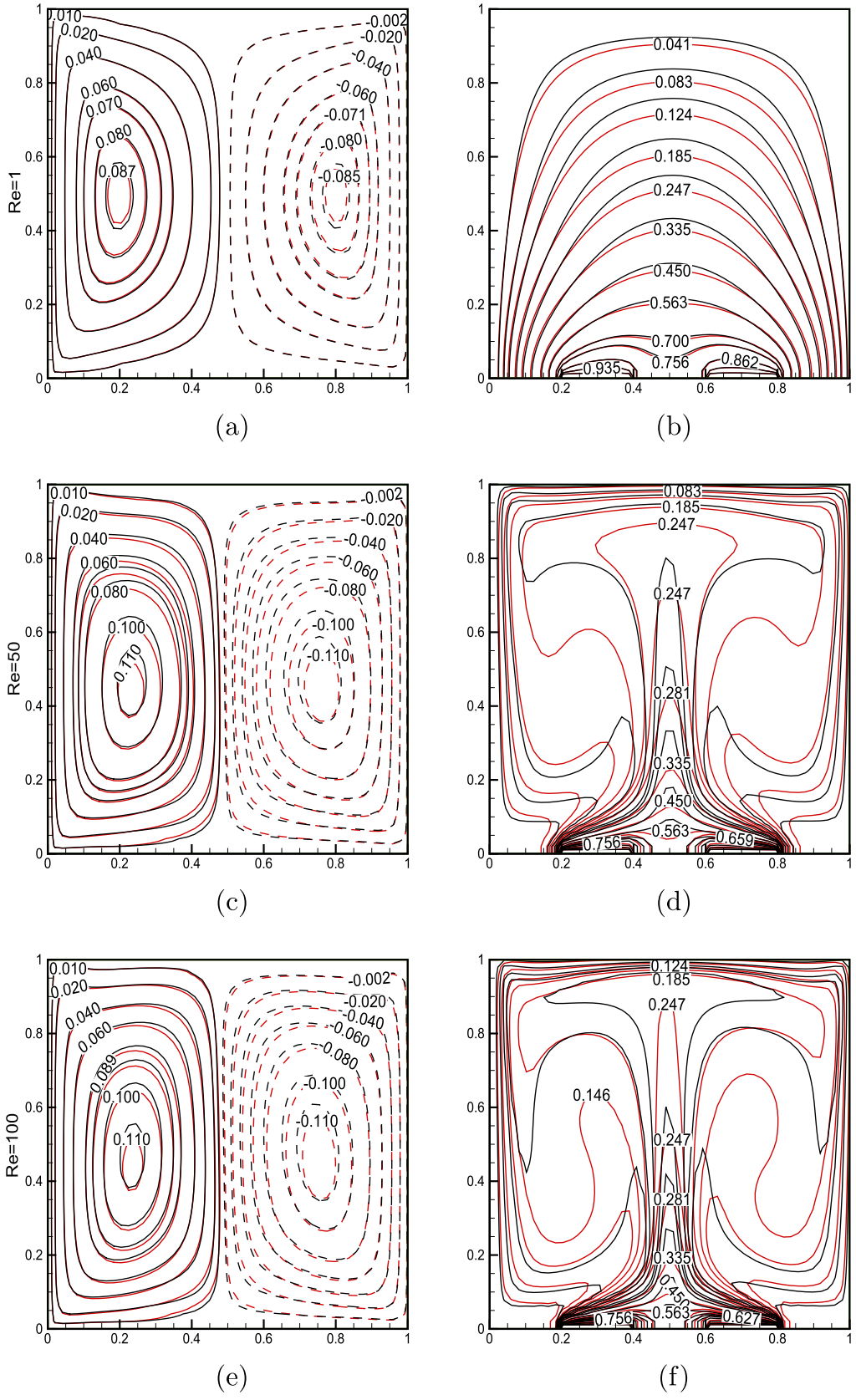

Fig. 8. Streamlines and isotherm lines of clear fluid ($\phi = 0.0$, Black) and nanofluid ($\phi = 0.2$, Red) at $Ri = 10$, $1 \leqslant Re \leqslant 100$ for Case-III.

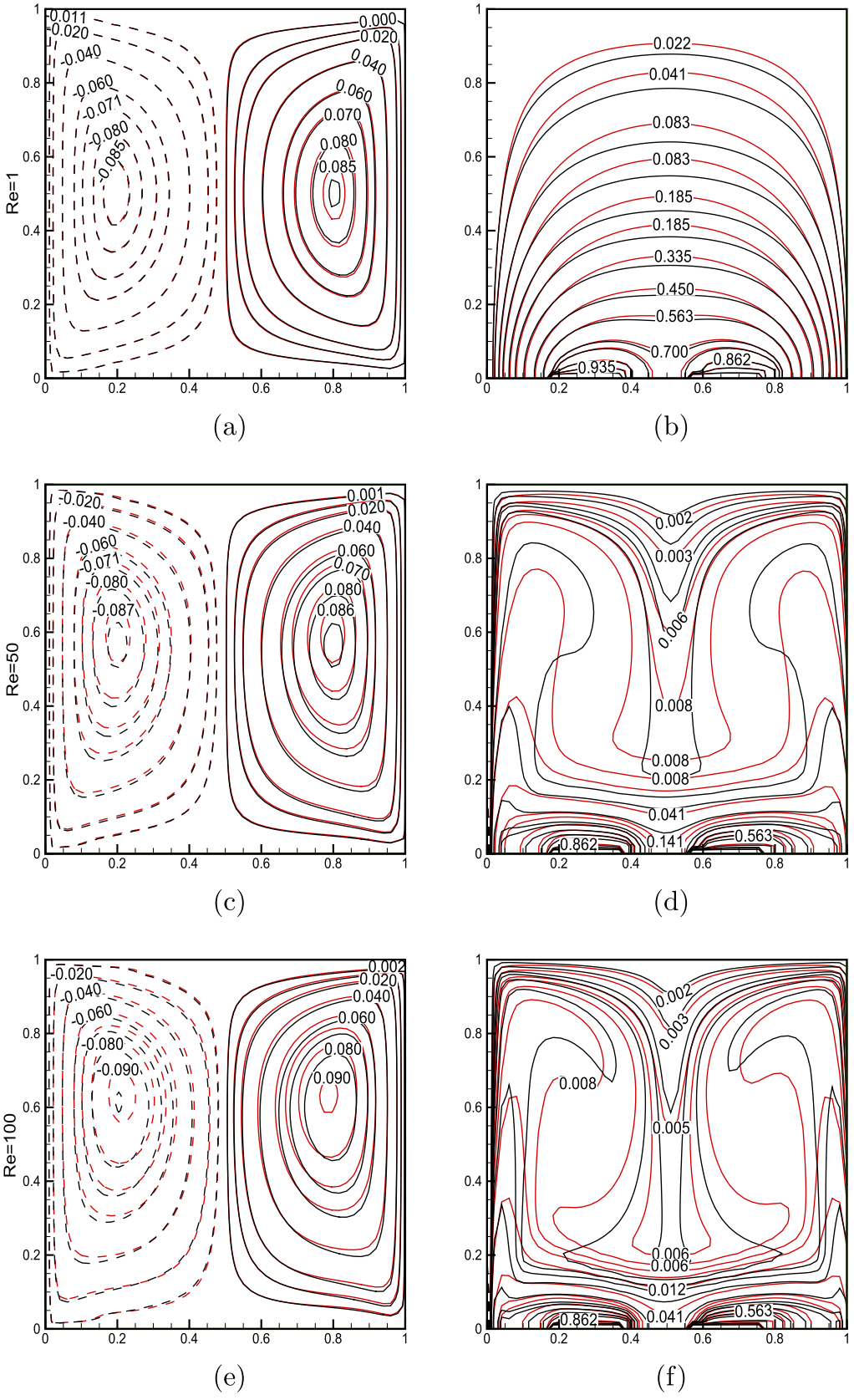

Fig. 9. Streamlines and isotherm lines of clear fluid ($\phi = 0.0$, Black) and nanofluid ($\phi = 0.2$, Red) at $Ri = 0.1$, $1 \leqslant Re \leqslant 100$ for Case-IV.

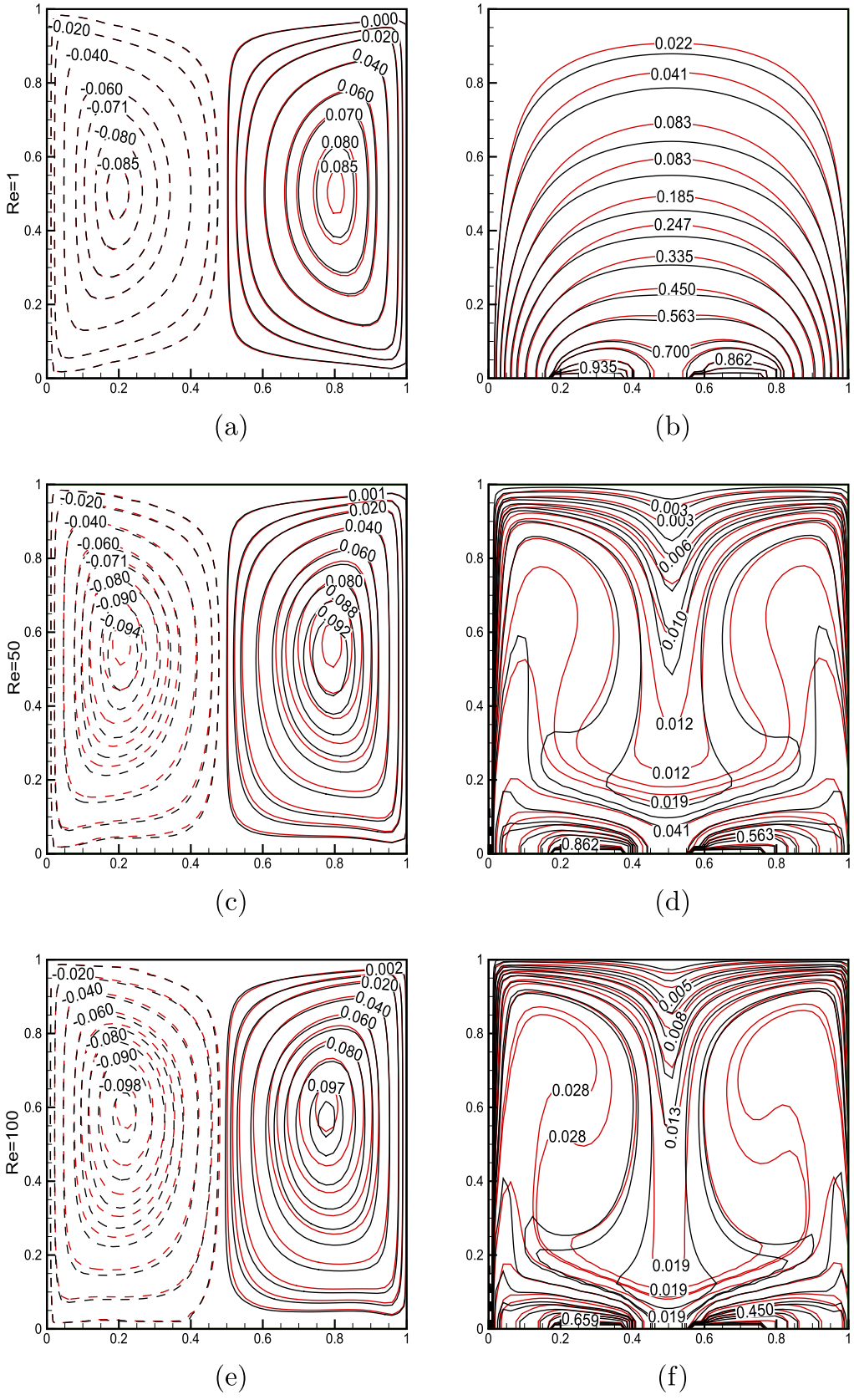

Fig. 10. Streamlines and isotherm lines of clear fluid ($\phi = 0.0$, Black) and nanofluid ($\phi = 0.2$, Red) at $Ri = 10$, $1 \leqslant Re \leqslant 100$ for Case-IV.

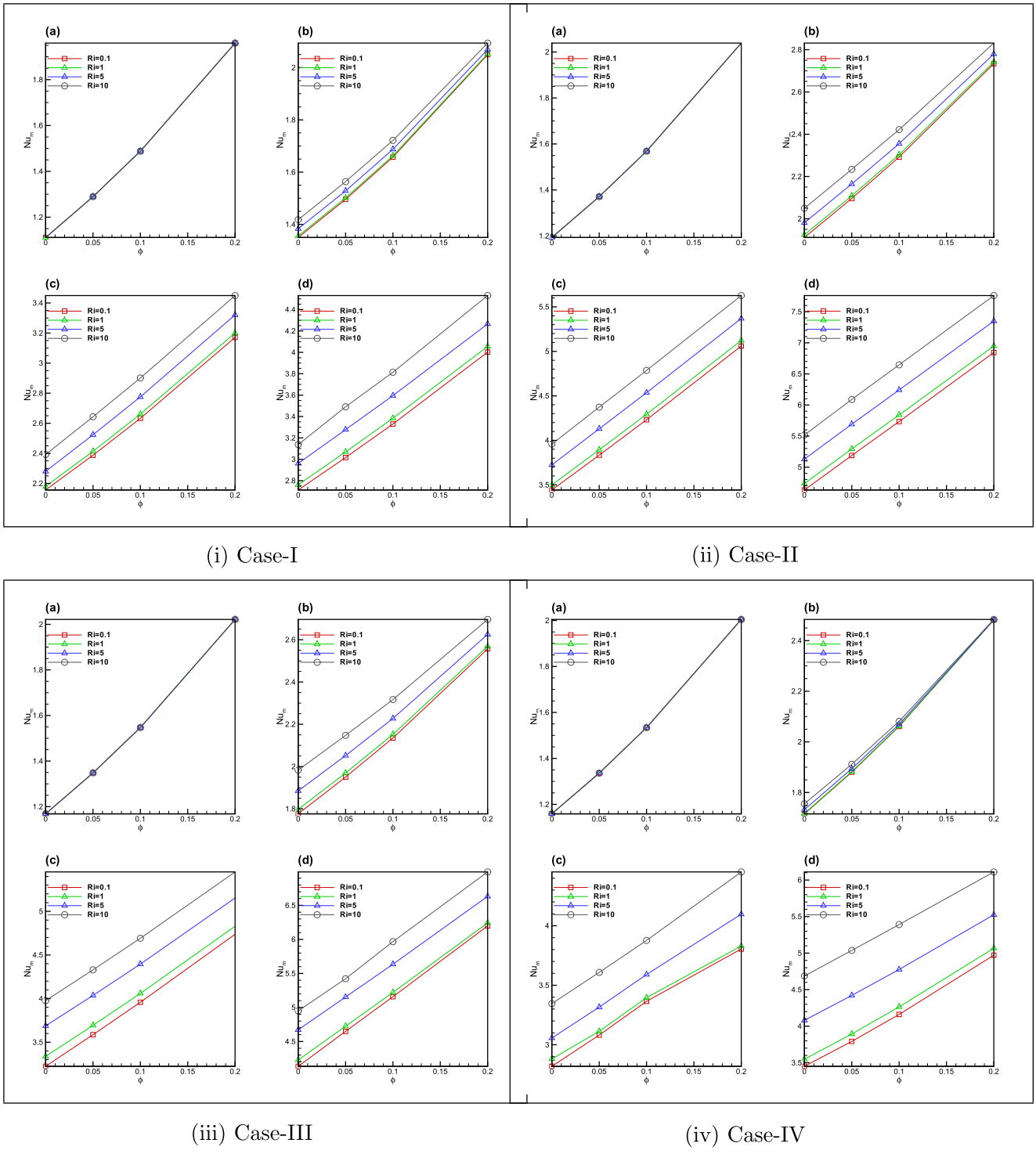

Fig. 11. Variation of average Nusselt number with respect to solid volume fraction of nanoparticles and Richardson number for different values of Reynolds number ((a) $Re = 1$, (b) $Re = 10$, (c) $Re = 50$ and (d) $Re = 100$) for Case-I to Case-IV.

6. Conclusion

This paper presents a comparative study of mixed convection flow in a two-dimensional lid driven square cavity filled with Cu–water nanofluid. The cavity is partially heated from below, using two discrete heat sources. The effect of solid volume fraction, Reynolds number and Richardson number and the direction lid movement on the fluid flow and heat transfer have been investigated numerically. From the above study, the conclusions are summarized as follows:

1. It is found that the heat transfer and fluid flow is sensitive to the solid volume fraction. Moreover, the solid volume fraction variation is an active factor for the average Nusselt number as nanoparticle volume fraction changes flow pattern.
2. The physical flow parameter Ri is mostly affecting the heat transfer rate. When $Ri < 1$, the results predicted that the flow and heat transfer is dominated by forced convection effect and when $Ri > 1$, flow and heat transfer are dominated by natural convection.

3. For a constant solid volume fraction with the increase of *Re* and *Ri*, it is found that heat transfer increases irrespective of the direction of moving walls. Out of the four given cases, the maximum heat transfer is found in Case-II. But, for $Ri < 0.1$ the result does not hold.
4. The solid volume fraction is found to be most effective in Case-I as the increment in average Nusselt number is found to be best for all *Ri* but still the overall heat transfer is minimum in this case as the average Nusselt number values are minimum as compared to other cases. The maximum heat transfer is obtained in Case-II, as in this case the average Nusselt number values for all parameters are maximum.
5. The average rate of heat transfer has a sharp variation in Case-IV for large *Ri* and *Re* as the strength of the circulation is decreasing by the lid opposing buoyancy forces.

Acknowledgement

The authors are thankful to the referees for their valuable comments, which enabled to present an improved version of the paper. Author Sumit Malik, is grateful to MHRD India and Dr. A.K. Nayak is thankful to SERB (under DST financed by Project no. SR/S4/MS: 765/12) India for providing financial support during the preparation of this manuscript.

References

[1] S.U.S. Choi, Enhancing thermal conductivity of fluids with nanoparticles, ASME Fluids Eng. Div. 231 (1995) 99–105.
[2] K. Khanafer, K. Vafai, M. Lightstone, Buoyancy driven heat transfer enhancement in a two-dimensional enclosure utilizing nanofluids, Int. J. Heat Mass Transfer 46 (2003) 3639–3653, http://dx.doi.org/10.1016/S0017-9310(03)00156-X.
[3] A.R.A. Khaled, K. Vafai, Heat transfer enhancement through control of thermal dispersion effects, Int. J. Heat Mass Transfer 48 (2005) 2172–2185, http://dx.doi.org/10.1016/j.ijheatmasstransfer.2004.12.035.
[4] S.E.B. Maiga, S.J. Palm, C.T. Nguyen, G. Roy, N. Galanis, Heat transfer enhancement by using nanofluids in forced convection flows, Int. J. Heat Fluid Flow 26 (2005) 530–546, http://dx.doi.org/10.1016/j.ijheatfluidflow.2005.02.004.
[5] R.K. Tiwari, M.K. Das, Heat transfer augmentation in a two-sided lid-driven differentially heated square cavity utilizing nanofluids, Int. J. Heat Mass Transfer 50 (2007) 2002–2018, http://dx.doi.org/10.1016/j.ijheatmasstransfer.2006.09.034.
[6] C.T. Nguyen, F. Desgranges, G. Roy, N. Galanis, T. Mare, S. Boucher, H. Angue Minsta, Temperature and particle-size dependent viscosity data for waterbased nanofluids – hysteresis phenomenon, Int. J. Heat Fluid Flow 28 (2007) 1492–1506, http://dx.doi.org/10.1016/j.ijheatfluidflow.2007.02.004.
[7] H. Angue Minsta, G. Roy, C.T. Nguyen, D. Doucet, New temperature and conductivity data for water-based nanofluids, Int. J. Therm. Sci. 48 (2009) 363–371, http://dx.doi.org/10.1016/j.ijthermalsci.2008.03.009.
[8] M. Muthtamilselvan, P. Kandaswamy, J. Lee, Heat transfer enhancement of copper-water nanofluids in a lid-driven enclosure, Commun. Nonlinear Sci. Numer. Simul. 15 (6) (2010) 1501–1510, http://dx.doi.org/10.1016/j.cnsns.2009.06.015.
[9] E. Abu-Nada, Z. Masoud, H. Oztopd, A. Campo, Effect of nanofluid variable properties on natural convection in enclosures, Int. J. Thermal Sci. 49 (2010) 479–491, http://dx.doi.org/10.1016/j.ijthermalsci.2009.09.002.
[10] A.A. Abbasian Arani, S.M. Sebdani, M. Mahmoodi, A. Ardeshiri, M. Aliakbari, Numerical study of mixed convection flow in a lid-driven cavity with sinusoidal heating on side walls using nanofluid, Superlattices Microstruct. 51 (2012) 893–911, http://dx.doi.org/10.1016/j.spmi.2012.02.015.
[11] F. Talebi, A.H. Mahmoudi, M. Shahi, Numerical study of mixed convection flows in a square lid-driven cavity utilizing nanofluid, Int. Commun. Heat Mass Transfer 37 (2010) 79–90, http://dx.doi.org/10.1016/j.icheatmasstransfer.2009.08.013.
[12] A.H. Mahmoudi, M. Shahi, F. Talebi, Effect of inlet and outlet location on the mixed convective cooling inside the ventilated cavity subjected to an external nanofluid, Int. Commun. Heat Mass Transfer 37 (2010) 1158–1173, http://dx.doi.org/10.1016/j.icheatmasstransfer.2010.04.004.
[13] F. Selimefendigil, H.F. Oztop, Natural convection and entropy generation of nanofluid filled cavity having different shaped obstacles under the influence of magnetic field and internal heat generation, J. Taiwan Inst. Chem. Eng. 56 (2015) 42–56, http://dx.doi.org/10.1016/j.jtice.2015.04.018.
[14] F. Selimefendigil, H.F. Oztop, K. Al-Salem, Natural convection of ferrofluids in partially heated square enclosures, J. Magn. Magn. Mater. 372 (2014) 122–133, http://dx.doi.org/10.1016/j.jmmm.2014.07.058.
[15] F. Selimefendigil, H.F. Oztop, MHD mixed convection of nanofluid filled partially heated triangular enclosure with a rotating adiabatic cylinder, J. Taiwan Inst. Chem. Eng. 45 (2014) 2150–2162, http://dx.doi.org/10.1016/j.jtice.2014.06.018.
[16] F. Selimefendigil, H.F. Oztop, Numerical investigation and reduced order model of mixed convection at a backward facing step with a rotating cylinder subjected to nanofluid, Comput. Fluids 109 (2015) 27–37, http://dx.doi.org/10.1016/j.compfluid.2014.12.007.
[17] F. Selimefendigil, H.F. Oztop, Effects of phase shift on the heat transfer characteristics in pulsating mixed convection flow in a multiple vented cavity, Appl. Math. Model. 39 (2015) 3666–3677, http://dx.doi.org/10.1016/j.apm.2014.11.065.
[18] F. Selimefendigil, H.F. Oztop, Pulsating nanofluids jet impingement cooling of a heated horizontal surface, Int. J. Heat Mass Transfer 69 (2014) 54–65, http://dx.doi.org/10.1016/j.ijheatmasstransfer.2013.10.010.
[19] F. Selimefendigil, H.F. Oztop, Numerical study of MHD mixed convection in a nanofluid filled lid driven square enclosure with a rotating cylinder, Int. J. Heat Mass Transfer 78 (2014) 741–754, http://dx.doi.org/10.1016/j.ijheatmasstransfer.2014.07.031.
[20] F. Selimefendigil, H.F. Oztop, Mixed convection of ferrofluids in a lid driven cavity with two rotating cylinders, Eng. Sci. Technol. Int. J. 18 (2015) 439–451, http://dx.doi.org/10.1016/j.jestch.2015.03.003.
[21] F. Selimefendigil, H.F. Oztop, Mixed convection in a two-sided elastic walled and SiO2 nanofluid filled cavity with internal heat generation: effects of inner rotating cylinder and nanoparticle's shape, J. Mol. Liq. 212 (2015) 509–516, http://dx.doi.org/10.1016/j.molliq.2015.09.037.
[22] F. Selimefendigil, H.F. Oztop, Mixed convection due to rotating cylinder in an internally heated and flexible walled cavity filled with SiO_2.water nanofluids: effect of nanoparticle shape, Int. Commun. Heat Mass Transfer 71 (2016) 9–19, http://dx.doi.org/10.1016/j.icheatmasstransfer.2015.12.007.
[23] F. Selimefendigil, H.F. Oztop, MHD mixed convection and entropy generation of nanofluid filled lid driven cavity under the influence of inclined magnetic fields imposed to it supper and lower diagonal triangular domains, J. Magn. Magn. Mater. 406 (2016) 266–281, http://dx.doi.org/10.1016/j.jmmm.2016.01.039.
[24] F. Garoosi, L. Jahanshaloo, M.M. Rashidi, A. Badakhsh, M.E. Ali, Numerical simulation of natural convection of the nanofluid in heat exchangers using a Buongiorno model, Appl. Math. Comput. 254 (2015) 183–203, http://dx.doi.org/10.1016/j.amc.2014.12.116.
[25] S.M. Sebdani, M. Mahmoodi, S.M. Hashemi, Effect of nanofluid variable properties on mixed convection in a square cavity, Int. J. Thermal Sci. 52 (2012) 112–126, http://dx.doi.org/10.1016/j.ijthermalsci.2011.09.003.
[26] F. Garoosi, S. Garoosi, K. Hooman, Numerical simulation of natural convection and mixed convection of the nanofluid in a square cavity using Buongiorno model, Powder Technol. 268 (2014) 279–292, http://dx.doi.org/10.1016/j.powtec.2014.08.006.
[27] F. Garoosi, L. Jahanshaloo, S. Garoosi, Numerical simulation of mixed convection of the nanofluid in heat exchangers using a Buongiorno model, Powder Technol. 269 (2015) 296–311, http://dx.doi.org/10.1016/j.powtec.2014.09.009.
[28] J.C. Maxwell, A Treatise on Electricity and Magnetism, second ed., Oxford University Press, Cambridge, 1904. 435–441.
[29] H.C. Brinkman, The viscosity of concentrated suspensions and solutions, J. Chem. Phys. (4) (1952) 571–581, http://dx.doi.org/10.1063/1.1700493.
[30] S.V. Patankar, Numerical Heat Transfer and Fluid Flow, Hemisphere, Washington, DC, 1980.
[31] H. Moumni, H. Welhezi, R. Djebali, E. Sediki, Accurate finite volume investigation of nanofluid mixed convection in two-sided lid driven cavity including discrete heat sources, Appl. Math. Model. 39 (14) (2015) 4164–4179, http://dx.doi.org/10.1016/j.apm.2014.12.035.
[32] F. Garoosi, G. Bagheri, M.M. Rashidi, Two phase simulation of natural convection and mixed convection of the nanofluid in a square cavity, Powder Technol. 275 (2015) 239–256, http://dx.doi.org/10.1016/j.powtec.2015.02.013.
[33] F. Garoosi, B. Rohani, M.M. Rashidi, Two-phase mixture modeling of mixed convection of nanofluids in a square cavity with internal and external heating, Powder Technol. 275 (2015) 304–321, http://dx.doi.org/10.1016/j.powtec.2015.02.015.
[34] F. Garoosi, G. Bagheri, F. Talebi, Numerical simulation of natural convection of nanofluids in a square cavity with several pairs of heaters and coolers (HACs) inside, Int. J. Heat Mass Transfer 67 (2013) 362–376, http://dx.doi.org/10.1016/j.ijheatmasstransfer.2013.08.034.
[35] F. Garoosi, F. Hoseininejad, Numerical study of natural and mixed convection heat transfer between differentially heated cylinders in an adiabatic enclosure filled with nanofluid, J. Mol. Liq. 215 (2016) 1–17, http://dx.doi.org/10.1016/j.molliq.2015.12.016.
[36] H.F. Oztop, I. Dagtekin, Mixed convection in two-sided lid-driven differentially heated square cavity, Int. J. Heat Mass Transfer 47 (8–9) (2004) 1761–1769, http://dx.doi.org/10.1016/j.ijheatmasstransfer.2003.10.016.